Comparison of Open-Hole Compression Strength and Compression After Impact Strength on Carbon Fiber/Epoxy Laminates for the Ares I Composite Interstage

A.J. Hodge, A.T. Nettles, and J.R. Jackson
Marshall Space Flight Center, Marshall Space Flight Center, Alabama

ii

Available from:

NASA Center for AeroSpace Information
7115 Standard Drive
Hanover, MD 21076–1320
443–757–5802

This report is also available in electronic form at
<https://www2.sti.nasa.gov/login/wt/>

ii

TABLE OF CONTENTS

LIST OF FIGURES

LIST OF FIGURES (Continued)

LIST OF TABLES

LIST OF ACRONYMS AND SYMBOLS

Al	aluminum
CAI	compression after impact
FEP	fluorinated ethylene propylene
IRT	infrared thermography
NDE	nondestructive evaluation
OHC	open-hole compression
OML	outer mold line
PAUT	passed array ultrasonic testing
UT	ultrasonic test

NOMENCLATURE

a_o average stress criterion characteristic distance

d_o point stress criterion characteristic distance

E_L longitudinal modulus of elasticity

E_T transverse modulus of elasticity

G_{LT} shear modulus

k_T stress concentration factor

x impact energy

β_0 regression constant

β_1 regression coefficient

ν_{LT} Poisson's ratio

σ_r residual stress

TECHNICAL PUBLICATION

COMPARISON OF OPEN-HOLE COMPRESSION STRENGTH AND COMPRESSION AFTER IMPACT STRENGTH ON CARBON FIBER/EPOXY LAMINATES FOR THE ARES I COMPOSITE INTERSTAGE

1. INTRODUCTION

Mechanical testing of representative subelements of the Ares I composite interstage was performed as part of the development of damage tolerance strength allowables and a damage threat assessment. Properties obtained included compression after impact (CAI), notched compression, and compression with simulated delaminations. The results were used to assess the damage tolerance of the interstage design and establish thresholds for inspection. This Technical Publication compares the compression strength results from various impact energy levels and impactor geometries to the compression results of various notch and delamination sizes.

A failure prediction model of 'notched' composite laminates (i.e., laminates with a stress riser) has been an endeavor pursued for many years. Notches from holes or impact damage in a laminate are more detrimental to compression strength than the tensile strength.[1–6] In the 1970s, Whitney and Nuismer provided the average stress and point stress failure criteria for notched laminates based upon fracture toughness criteria.[7] Originally developed for notched tension, this method has successfully been applied to notched compression. The stress concentration factor k_T is used in conjunction with a characteristic distance for the two criteria for the laminate to fit a curve to empirically derived data (fig.1). In the point stress criterion, failure occurs when the stress at a distance d_o away from the hole reaches the unnotched material strength σ_o. In the average stress criterion, failure occurs when the average stress over the distance a_o reaches σ_o. It was originally hoped that the characteristic distance parameters would be universal constants for all fibrous material systems and all layups. However, it has been shown that these values are dependent upon many factors including hole size and stacking sequence.[8] Notwithstanding, the simplicity of application of the Whitney-Nuismer model adds appeal to any user and this predictive model is described in most textbooks. In the 1990s, Soutis et al. developed a cohesive zone model for predicting open-hole compression (OHC) strength based upon the kink band formation in zero-degree plys within the laminate.[9] The model was further refined to predict CAI strength. Other researchers have continued to refine these approaches. Chen et al. modified the Whitney average stress criterion to calculate a characteristic length for tension and compression.[10] The model agreed well for all laminates tested except those with a high percentage of zero-degree plys. Callus compared the point and average stress criterion models with a cohesive zone model.[11] The average stress criterion and cohesive zone model were almost identical for hole sizes zero to 0.25 in.
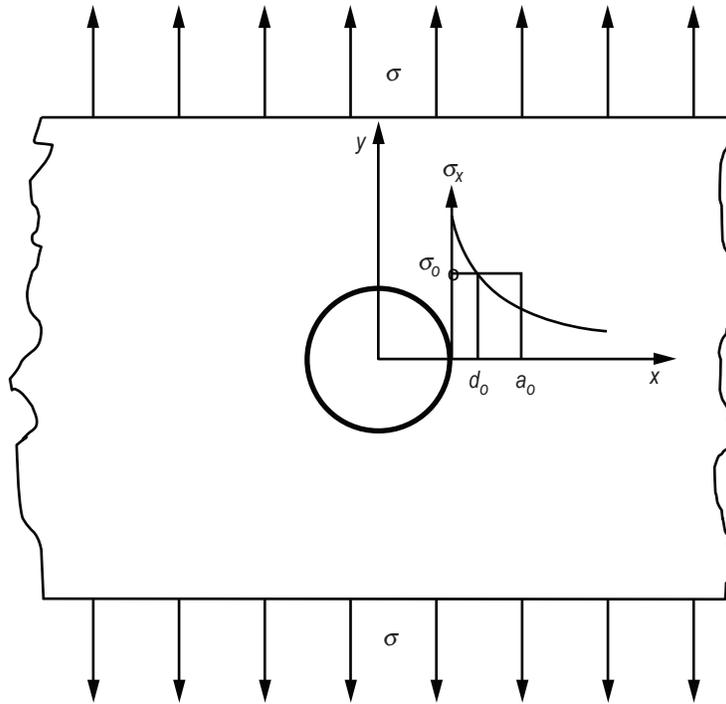
Figure 1. Schematic of stress distribution near a hole with characteristic distance (d_o and a_o) as applicable to the point and average stress criterion.

Other researchers have made comparisons between the strength reductions of OHC and CAI. Byers (1980) found that impact damage size measured by ultrasonic through transmission was not a good predictor of residual strength and did not correlate well with OHC, while Williams (1984) found similar reductions in strength between OHC and CAI strengths for a given damage size.[12,13] More recently, Chen modeled CAI residual strength as an eliptical hole on the assumption of similar failure mechanisms; however, Edgren et al. concluded that modeling impact damage as an open hole was not valid.[14,15] Clearly, the study of compressive failure mechanisms of notched laminates is an area of intense study.

A major disadvantage of any of these failure criteria is the reliance on an accurate empirical measurement of unnotched strength. Unnotched strength is dependent upon test method, specimen geometry, and quality of specimen preparation. The models described above can alternately be utilized to predict unnotched strength when notched strength is known. This raises the question: "Why normalize to unnotched strength?" Strength allowables consist of reduction factors, or knockdowns, for discontinuities, notches, process variability, and damage such that a well-designed structure would never be loaded to pristine, unnotched strength values. Providing an unnotched strength allowable may in fact be detrimental to the design process by suggesting that such capability is achievable. Decisions and analyses become anchored to this irrelevant value rather than a value relevant to the design function of a composite structure.

2. MATERIALS AND TESTING

Face sheets in this study were composed of IM7/8552-1 140 g/m^2 areal weight fiber placed ribbon. The acreage design of the Ares I upper stage interstage consisted of thin laminates with a (45,0,–45,0,90,0,0,90,0)$_s$ layup on each face sheet. Thick laminates represented buildups for high stress regions and were 40- and 56-ply quasi-isotropic. Acreage sections were co-cured onto 1.5-in-thick 5052 aluminum (Al) honeycomb core with 1/8-in cell size on two densities of core—3.1 and 6.1 lb/ft^3. Processing problems were encountered with the lighter core material which included face sheet wrinkling and core crushing during autoclave cure. Thus, only the 6.1 lb/ft^3 results are examined. Forty-ply face sheet laminates were only fabricated with 6.1 lb/ft^3 core. Fifty-six-ply face sheets were co-cured onto 1.5-in-thick, 12 lb/ft^3 Al core. It was later found that the large coefficient of thermal expansion mismatch between the 12 lb/ft^3 core and the carbon fiber face sheets led to core node disbonds during cooldown on two of the three batches of core. Face sheets were bonded to the core with 0.08 lb/ft^2 FM300K film adhesive at 355 °F with a 55 lb/in^2 autoclave pressure.

Three series of tests were conducted: CAI, OHC, and compression with simulated delamination. Delaminations were simulated with two layers of 0.001-in-thick fluorinated ethylene propylene (FEP) tape inserted within the face sheet during layup. The OHC specimens were not sandwich panels, but were instead monolithic laminates cured at the same pressure as the sandwich panels.

The raw test data for the mechanical tests are available in appendix A.

2.1 Compression After Impact

Impact testing was performed with three different impactor diameters (0.25, 0.5, and 1.5 in). Sandwich specimens (4 in wide by 6 in long) were impacted over a range of impact energies such as to cause damage ranges not visible to face sheet penetration. Post-impact damage sizes were obtained with nondestructive evaluation (NDE). Thin face sheet specimens were evaluated with infrared thermography (IRT) and thick face sheet specimens were evaluated with passed array ultrasonic testing (PAUT). The length and width of the NDE indication was noted for each specimen. Figure 2 illustrates the damage width indicated by NDE compared to the impact energy and impactor size. The 0.25-in-diameter impacting tup began to penetrate at 10 ft-lb with full penetration of the face sheet at 12 ft-lb. The 0.5-in-diameter tup began to penetrate the face sheet at 15 ft-lb. The 1.5-in-diameter tup did not penetrate the face sheet at the impact energies applied and produced little visible damage other than a dent. It is apparent from figure 1 that damage size is a function of impactor size, especially between the 0.5- and 1.5-in-diameter impactors.
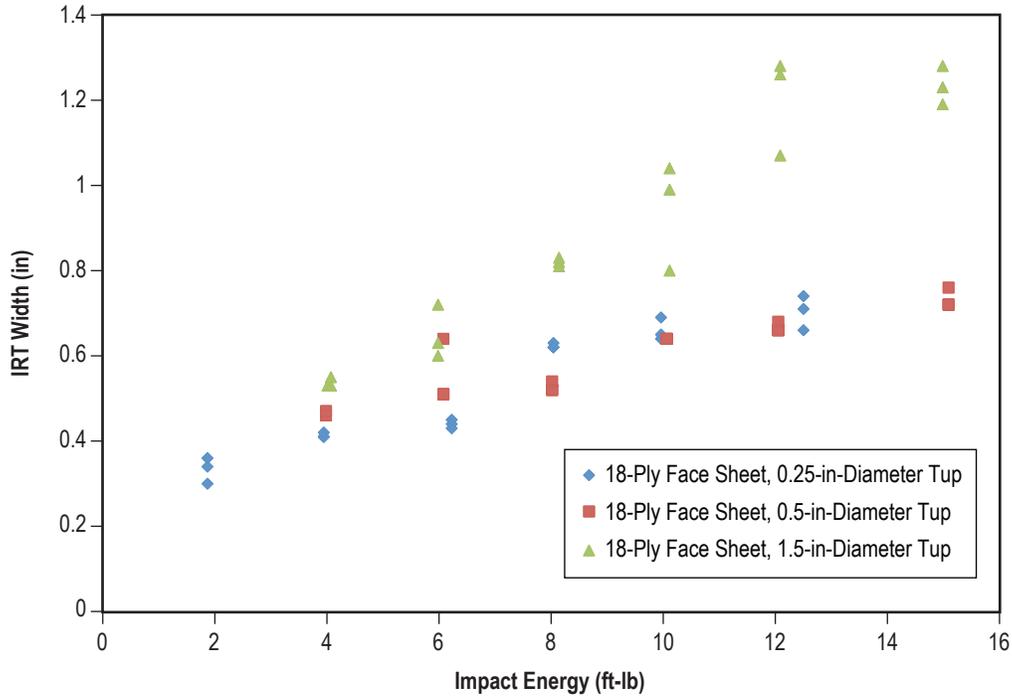
Figure 2. NDE indication width versus impact energy.

CAI specimens were then potted with epoxy into a 1-in-thick Al frame on each loading end. The loading ends were machined flat and parallel to within 0.001 in. Strain gages were bonded to the front and back surfaces away from the damage zone to monitor alignment during mechanical testing. Figure 3 is a schematic of the edgewise compression test.
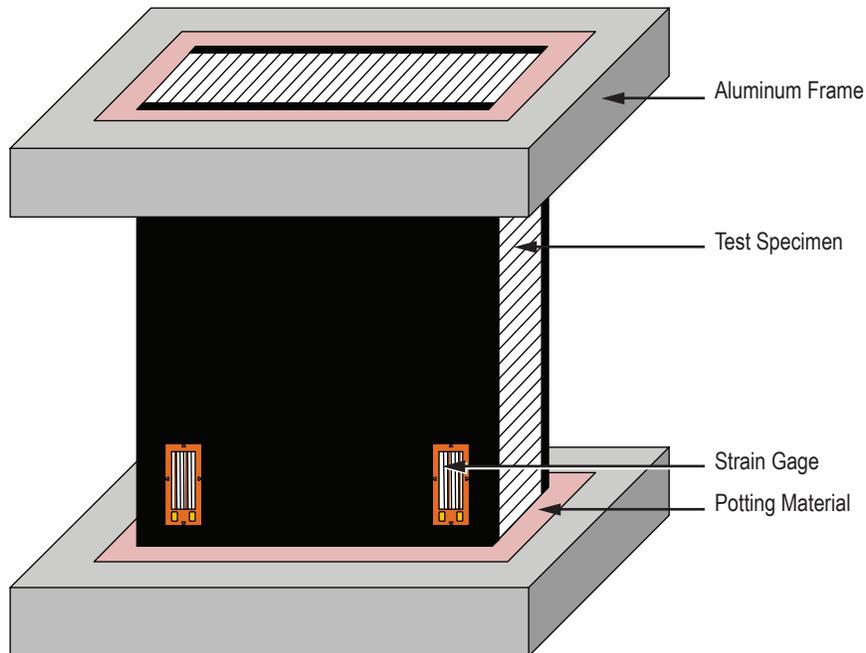
Figure 3. Sandwich edgewise compression.

4

In order to apply a uniform strain to both face sheets, the compression platens were fixed. The impacted sandwich specimens were loaded in edgewise compression at a constant crosshead rate until failure. Figures 4 and 5 illustrate the residual compression strength as compared to impact energy and damage width for the three impactor sizes used. It is apparent that the residual strength is dependent upon the impact energy and is independent of the impactor sizes used in this study. However, the residual strength appears to reach a plateau for a given critical impact energy, even if the damage size increases (≈45,000 psi at 12 ft-lb for the data presented here).
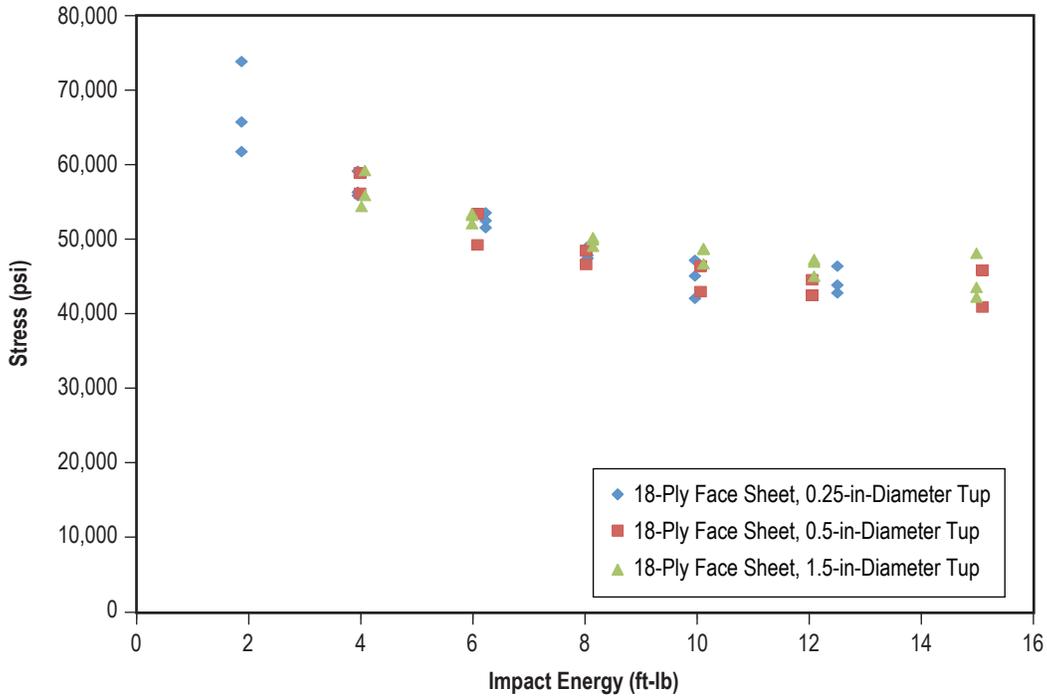
Figure 4. Residual compression strength versus impact energy.
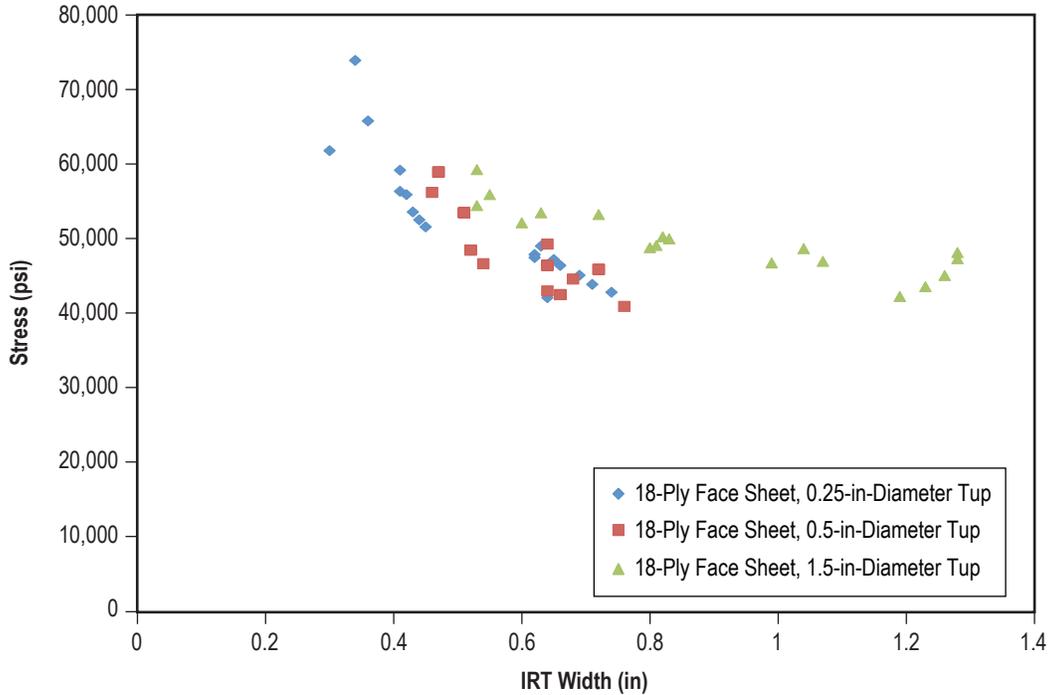
Figure 5. Residual compression strength versus NDE indication size.

2.2 Open-Hole Compression

OHC testing was performed on 18-ply flat laminates with the Northrop OHC test fixture and the Boeing CAI fixture. Figures 6 and 7 are schematics of the two fixtures. The Northrop fixture uses specimens 1 in wide by 3 in long. The Boeing fixture, also known as ASTM D7137, Standard Test Method for Compressive Residual Strength Properties of Damaged Polymer Matrix Composite Plates, utilized 4 in wide by 6 in long specimens.[17]

Three layups were tested: 18-ply orthotropic, 16-ply quasi-isotropic, and 32-ply unidirectional. The 18-ply and unidirectional laminates were tested in both the axial and transverse direction, making a total of five configurations. The 18-ply axially oriented coupons had the majority of fibers oriented in the loading direction with (56/22/22) representing the percentage of plies in the 0-, 45-, and 90-deg orientations. The 18-ply transverse specimens had a layup of (22/22/56). Quasi-isotropic specimens (25/50/25) were tested for comparison to the highly oriented laminates. Specimens with hole sizes ranging from 0.03125 to 1.32 in were tested. The zero-degree unidirectional coupons initially failed by in-plane shear parallel to the fibers at the hole edges prior to compressive failure. Thus, the ultimate failure strength showed no notch sensitivity since the test is reduced to a net section compression test. Because of the dual failure mode, the zero-degree data are not included in the figures. The 90-deg unidirectional coupons exhibited a much smaller notch sensitivity than the laminates. Figure 8 illustrates the OHC strength results for 1-in-wide coupons. As noted, prior researchers found both the cohesive zone model and average stress criterion to adequately fit OHC strength. The average stress criterion is shown as the solid lines in figure 8.

6
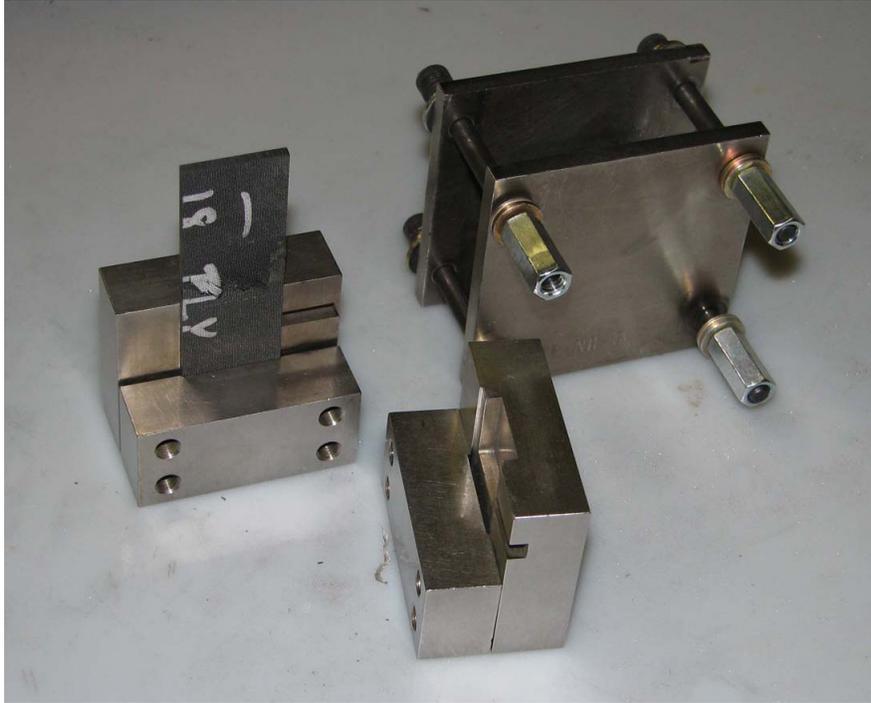
Figure 6. Northrop OHC fixture.[16]
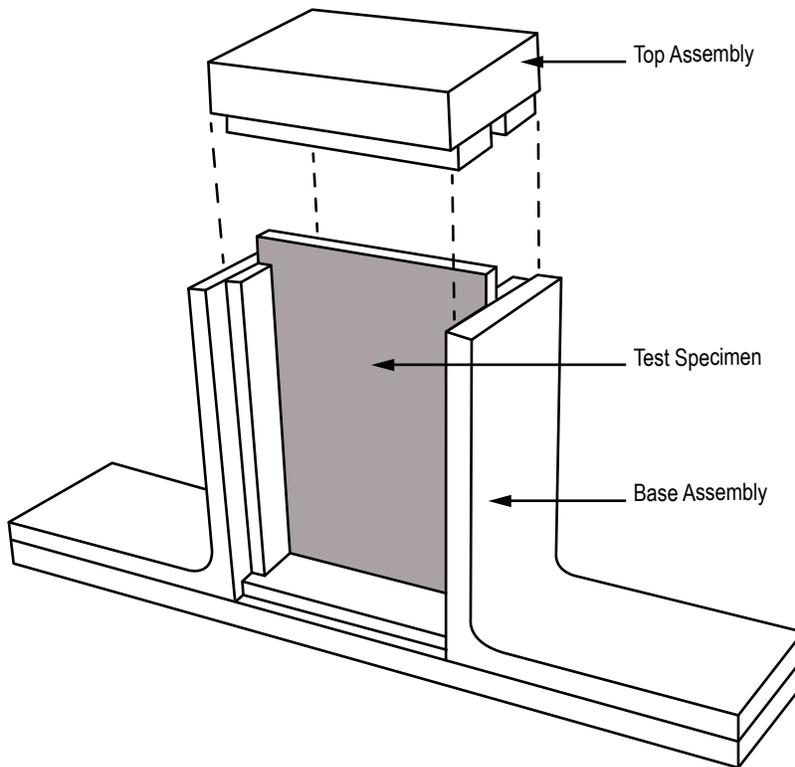
Figure 7. Boeing CAI fixture.[17]

7
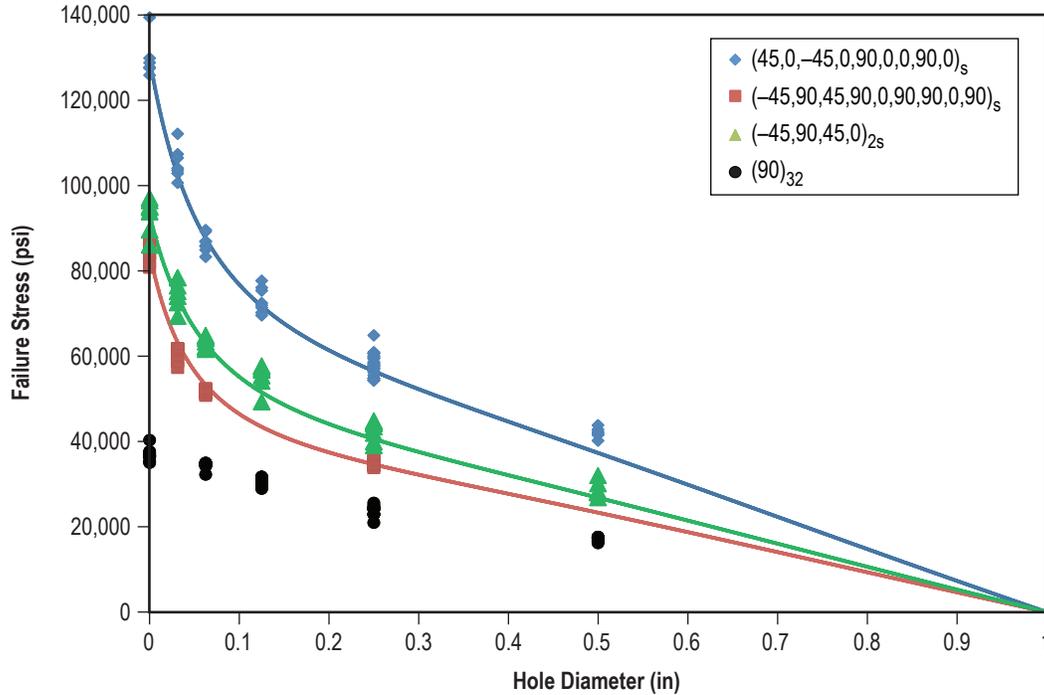
Figure 8. Laminate OHC results.

When considering fitting the OHC results to a predictive model, one must account for the parameters that may be adjusted to fit the data. Past researchers have adjusted the characteristic distance parameter to change the tensile model to a compressive model. The stress concentration factor was determined analytically from the elastic properties obtained through classical lamination theory and the following:

$$k_T = 1 + \sqrt{2\left(\sqrt{\frac{E_L}{E_T}} - v_{LT}\right) + \frac{E_L}{G_{LT}}} \quad . \tag{1}$$

A finite width correction factor as described in Carlsson and Pipes was employed.[18] It was found that using the same characteristic distance for three different layups did not adequately model the data. Furthermore, the average stress criterion best fit all three layups when a constant stress concentration factor was used, rather than adjusting based upon elastic properties as calculated from equation (1). The only way all three layups could be fit to the average stress criterion was to adjust the stress concentration factor and the characteristic distance parameters.

When one considers all of the OHC strength values are fit to a model based on an unnotched strength, the importance of this parameter becomes apparent. It was found that if the OHC strength results are normalized to an arbitrary notch size (1/32 in, for example) the model then becomes predictive for unnotched strength. By removing the unnotched data from the equation, the predictive model can better fit the notched results of the three layups using only one stress concentration factor

8

and one characteristic distance (fig. 9). The line representing the average stress criterion utilizes a characteristic distance of 0.03 in and a stress concentration factor of 3.
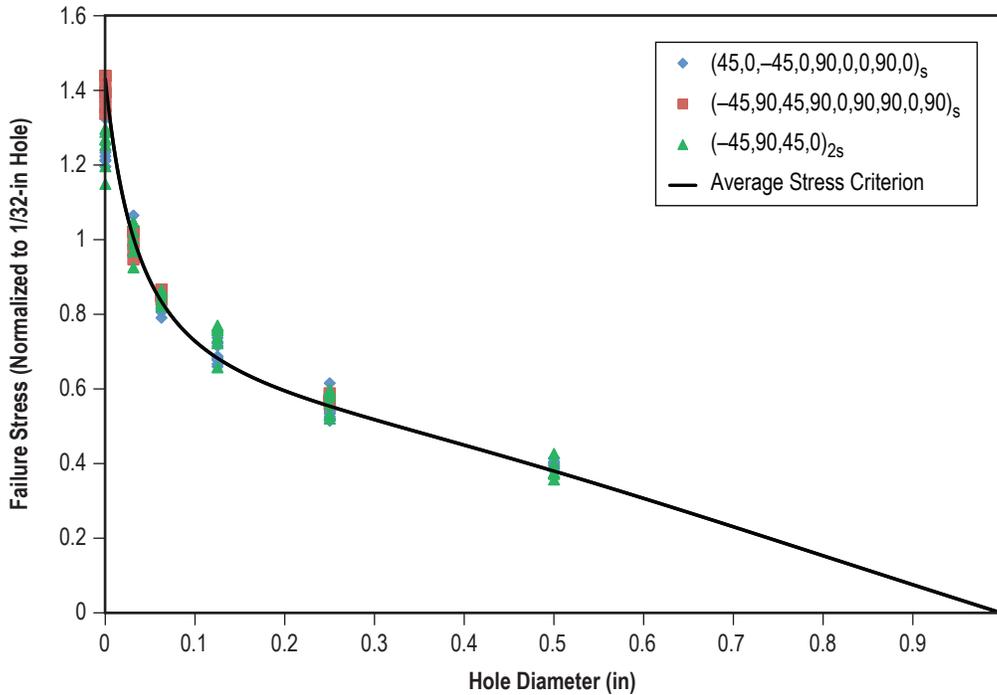
Figure 9. OHC normalized to 1/32-in-diameter hole.

As previously noted, normalizing the OHC strengths to the unnotched strength is dependent upon obtaining an accurate unnotched strength. A low test value for unnotched strength will provide low estimates for notched properties.

CAI residual strength has been successfully fitted with a power law of the expression: $\log(\sigma_r) = \beta_0 + \beta_1 \log(x)$, where σ_r is the residual stress, β_0 and β_1 are the regression constant and regression coefficient, respectively, from the population statistics, and x is the impact energy (or damage size in this study).[19–21] Interestingly, when the OHC strengths from this study were fitted with the power law, the curve fit better than with the average stress criterion for the 18-ply laminate. However, if the stress concentration factor for the 18-ply laminate is allowed to be adjusted, the average stress criterion could provide a better fit.

2.3 Testing of Simulated Delaminations and Unbonds

Delaminations and adhesive unbonds within the sandwich were simulated with a double layer of FEP tape. These panels were fabricated with hand layup using 12-in-wide prepreg rather than fiber placement. Three geometries of FEP tape were placed within the laminate: (1) A 1-in-diameter disk, (2) a 1-in square, and (3) a 2-in-long by 1-in-wide rectangle, where the length is perpendicular to the loading direction. Two different depths were examined: (1) Between the face sheet and core on

the bag side representing the outer mold line (OML) and (2) within the midplane of the face sheet on the OML side. The test results demonstrated that a delamination within the face sheet is much more detrimental to the compression strength than an unbond between the core and the face sheet. Table 1 shows the results of the sandwich edgewise compression testing with simulated delaminations and adhesive unbonds.

Table 1. Compression test results of sandwich defect coupons.

Defect Geometry	Defect Location	Failure Stress (lb/in^2)
1-in disk	Between face sheet and core	104,000
1-in disk	Center of OML face sheet	77,000
1-in square	Between face sheet and core	109,000
1-in square	Center of OML face sheet	70,000
1- $\times$ 2-in rectangular	Between face sheet and core	84,000
1- $\times$ 2-in rectangular	Center of OML face sheet	54,000
No defect	NA	101,000
0.25-in open hole	Center through hole	61,000
0.25-in open hole	Center through hole	65,000

2.4 Comparison of Impact Damage, Open-Hole Compression, and Delamination

When comparing the residual compression strength of the three types of stress risers as a function of defect size, it is obvious that the OHC bounds the CAI and the simulated delaminations. Figure 9 illustrates: (1) CAI strengths for the 18-, 40-, and the 56-ply sandwich coupons, (2) compression strength for the 18-ply simulated delamination sandwich coupons, and (3) the OHC strengths for the 18-ply laminate coupons. One issue with a comparison between the OHC and CAI results is the difference in structure. The OHC coupons were flat laminates and the CAI coupons were sandwich structure. Typically, laminates have a higher cure pressure than sandwich structures. However, for this study, all samples had the same cure pressure. A limited set of OHC was performed on the sandwich. Results compared well with the OHC laminate (see table 1 and fig. 10). The initial undamaged, or pristine, compression strength for the sandwich was lower than the undamaged strength for the laminate. This can be attributed to factors such as the dimpling of the face sheet during co-cure as well as the different test geometry. However, once a hole or impact damage was present, the notch seemed to overwhelm other factors.

2.5 Nondestructive Evaluation Size Correlation

The majority of dimensional measurements for delamination size were obtained by measurement of the IRT indication size. Thicker laminates; namely, the 56-ply quasi-isotropic laminate, used PAUT for the measurement of delamination size. To compare measurement techniques, 16 specimens were evaluated with both IRT and PAUT followed by cross-sectional analysis. The 18-ply sandwich specimens were impacted at ranges from 1 to 10 ft-lb with 0.5- and 1.5-in-diameter impactors. The 0.5-in-diameter impactor produced more visible damage than the 1.5-in-diameter impactor. However, the NDE indication was typically larger for the larger diameter indenter. The

Figure 10. Comparison of all defect types.

IRT and ultrasonic test (UT) methods correlated well as shown in tables 2 and 3. The cross-sectional measurement of damage size was typically the same or smaller than the damage size as measured by NDE methods. This can be explained because the cross section was often difficult to obtain at the exact center of the impact location, particularly for the lower energy impacts. The cross sections did show a difference in damage microstructure as illustrated in appendix B.

Table 2. Comparison of IRT, UT, and cross-sectional analysis for different impact energies with a 0.5-in-diameter impactor.

Impact Energy (ft-lb)	IRT Width (in)	UT Width (in)	Cross-Sectional Width (in)
0.8	0	0	0
1.8	0.53	0.56	0.425
2.6	0.62	0.59	0.55
3.6	0.66	0.65	0.55
5.4	0.75	0.80	0.74
7.2	0.75	0.89	0.84
9.1	0.89	1.00	0.9

11

Table 3. Comparison of IRT, UT, and cross-sectional analysis for different impact energies with a 1.5-in-diameter impactor.

Impact Energy (ft-lb)	IRT Width (in)	UT Width (in)	Cross-Sectional Width (in)
0.8	0	0	0
1.8	0.58	0.71	0.26
2.7	0.68	0.77	0.7
3.7	0.93	0.83	0.7
5.5	1.01	1.03	0.95
7.4	1.18	1.30	1.05
9.0	1.28	1.24	1.25
10.5	1.27	1.45	1.45

3. CONCLUSIONS

Given that the microstructure of damage induced by impact is dependent upon the size of the impactor, the validity of predicting residual strength primarily on damage area is questionable. Apparently, there are other factors influencing the residual strength other than the planar size of damage.

Impact energy was a better predictor of residual strength than NDE size. This conclusion holds regardless of the impactor sizes tested in this study. While the larger diameter impactor produced a larger NDE indication for a given impact energy, the residual strength was the same regardless of impactor size (see fig. 2). However, this affect also occurs where the residual strength begins to plateau. So, either method of strength prediction appear appropriate for the material examined in this study.

It was found that using a constant stress concentration factor of 3 provided better average stress criterion curve fits for the OHC strength data than when the calculated value from laminate elastic properties (eq. (1)) was used.

Some densities of core may be inappropriate for co-cure applications at the autoclave pressure used in this study. The lowest density core experienced core crushing in some instances. The highest density core exhibited node disbonds due to residual stresses induced during autoclave cooldown.

APPENDIX A—MECHANICAL TEST DATA

Table 4 includes the damage tolerance test results for the $(45,0,-45,0,90,0,0,90,0)_s$ 18-ply face sheet with 3.1 lb/ft^3 Al core. Only one panel was tested due to face sheet wrinkling and core crushing. Due to processing anomalies, it is not recommended to use such a thin foil thickness core with co-cure applications.

Table 4. 18-ply face sheet, 3.1 lb/ft^3 core damage tolerance results.

Sample Name	Tup Diameter (in)	Impact Energy (ft-lb)	IRT Width (in)	Failure Stress (psi)
AC-B1P3C3A-P1-A7-DT-1	0.5	1.53	0.2	69,548
AC-B1P3C3A-P1-A7-DT-2	0.5	3.49	0.27	49,308
AC-B1P3C3A-P1-A7-DT-3	0.5	4.74	0.33	46,686
AC-B1P3C3A-P1-A7-DT-4	0.5	6.32	0.37	43,576
AC-B1P3C3A-P1-A7-DT-5	0.5	8.81	0.44	38,421
AC-B1P3C3A-P1-A7-DT-6	0.5	9.51	0.44	41,494
AC-B1P3C3A-P1-A7-DT-7	0.5	3.75	0.18	54,882
AC-B1P3C3A-P1-A7-DT-8	0.5	5.49	0.55	52,870
AC-B1P3C3A-P1-A7-DT-9	0.5	7.34	0.59	46,869
AC-B1P3C3A-P1-A7-DT-10	0.5	9.24	0.69	45,029
AC-B1P3C3A-P1-A7-DT-11	0.5	11.08	0.69	45,163
AC-B1P3C3A-P1-A7-DT-12	0.5	13.85	0.83	45,486
AC-B1P3C3A-P1-A7-DT-13	0.5	3.33	0.4	64,533
AC-B1P3C3A-P1-A7-DT-14	0.5	5.64	0.55	50,023
AC-B1P3C3A-P1-A7-DT-15	0.5	7.38	0.7	52,364
AC-B1P3C3A-P1-A7-DT-16	0.5	9.10	0.9	48,152
AC-B1P3C3A-P1-A7-DT-17	0.5	11.10	0.99	46,659
AC-B1P3C3A-P1-A7-DT-18	0.5	13.84	1.08	50,426
AC-B1P3C3A-P1-A7-DT-19	0.5	1.71	0.3	64,358
AC-B1P3C3A-P1-A7-DT-20	0.5	9.00	0.77	–
AC-B1P3C3A-P1-A7-EC-10	0.5	3.60	0.4	–
AC-B1P3C3A-P1-A7-EC-11	0.5	3.68	0.44	–
AC-B1P3C3A-P1-A7-EC-12	0.5	8.78	0.44	–
AC-B1P3C3A-P1-A7-EC-13	0.5	9.15	0.46	–

Tables 5–8 include the damage tolerance test results for the $(45,0,-45,0,90,0,0,90,0)_s$ 18-ply with 6.1 lb/ft^3 Al core. Three sets of panels composed of three lots of core and three lots of film adhesive were fabricated in the same autoclave run. The face sheets for all three panels were from the same lot of material.

Table 5. 18-ply face sheet, 3.1 lb/ft^3 core damage tolerance results (batch 1).

Sample Name	Tup Diameter (in)	Impact Energy (ft-lb)	IRT Width (in)	Failure Stress (psi)
MDC-B1P1C1A-P1-A7-DT-1	0.25	1.55	0.34	73,927
MDC-B1P1C1A-P1-A7-DT-2	0.25	3.70	0.41	59,209
MDC-B1P1C1A-P1-A7-DT-3	0.25	5.97	0.43	53,612
MDC-B1P1C1A-P1-A7-DT-4	0.25	7.76	0.62	47,911
MDC-B1P1C1A-P1-A7-DT-5	0.25	9.72	0.64	42,125
MDC-B1P1C1A-P1-A7-DT-6	0.25	12.22	0.66	46,445
MDC-B1P1C1A-P1-A7-DT-7	0.5	3.82	0.47	58,968
MDC-B1P1C1A-P1-A7-DT-8	0.5	5.68	0.51	53,515
MDC-B1P1C1A-P1-A7-DT-9	0.5	7.21	0.52	48,512
MDC-B1P1C1A-P1-A7-DT-10	0.5	9.83	0.64	46,458
MDC-B1P1C1A-P1-A7-DT-11	0.5	11.63	0.66	42,537
MDC-B1P1C1A-P1-A7-DT-12	0.5	14.62	0.72	45,913
MDC-B1P1C1A-P1-A7-DT-13	1.5	4.30	0.53	54,477
MDC-B1P1C1A-P1-A7-DT-14	1.5	5.84	0.6	52,164
MDC-B1P1C1A-P1-A7-DT-15	1.5	7.92	0.83	50,017
MDC-B1P1C1A-P1-A7-DT-16	1.5	12.56	0.8	48,832
MDC-B1P1C1A-P1-A7-DT-17	1.5	10.98	1.07	46,997
MDC-B1P1C1A-P1-A7-DT-18	1.5	14.29	1.28	48,185
MDC-B1P1C1A-P1-A7-DT-19	NA	0.00	–	108,431*
MDC-B1P1C1A-P1-A7-EC-7	0.5	3.83	0.45	–
MDC-B1P1C1A-P1-A7-EC-9	0.5	3.84	0.53	–
MDC-B1P1C1A-P1-A7-EC-11	0.5	9.83	0.54	–
MDC-B1P1C1A-P1-A7-EC-13	0.5	9.83	0.61	–

* Failure by end brooming.

Table 6. 18-ply face sheet, 3.1 lb/ft^3 core damage tolerance results (batch 2).

Sample Name	Tup Diameter (in)	Impact Energy (ft-lb)	IRT Width (in)	Failure Stress (psi)
MDC-B1P2C2A-P1-A7-DT-1	0.25	1.63	0.3	61,829
MDC-B1P2C2A-P1-A7-DT-2	0.25	3.72	0.42	55,937
MDC-B1P2C2A-P1-A7-DT-3	0.25	5.97	0.44	52,557
MDC-B1P2C2A-P1-A7-DT-4	0.25	7.76	0.63	49,044
MDC-B1P2C2A-P1-A7-DT-5	0.25	9.77	0.69	45,132
MDC-B1P2C2A-P1-A7-DT-6	0.25	12.22	0.74	42,855
MDC-B1P2C2A-P1-A7-DT-7	0.5	3.81	0.52	56,301
MDC-B1P2C2A-P1-A7-DT-8	0.5	5.67	0.64	50,026
MDC-B1P2C2A-P1-A7-DT-9	0.5	7.64	0.58	50,190
MDC-B1P2C2A-P1-A7-DT-10	0.5	9.82	0.67	44,798
MDC-B1P2C2A-P1-A7-DT-11	0.5	12.62	0.72	42,685
MDC-B1P2C2A-P1-A7-DT-12	0.5	14.49	0.79	45,913
MDC-B1P2C2A-P1-A7-DT-13	1.5	4.02	0.55	55,949
MDC-B1P2C2A-P1-A7-DT-14	1.5	6.03	0.72	53,276
MDC-B1P2C2A-P1-A7-DT-15	1.5	7.92	0.82	50,290
MDC-B1P2C2A-P1-A7-DT-16	1.5	13.61	1.04	48,704
MDC-B1P2C2A-P1-A7-DT-17	1.5	13.66	1.26	45,102
MDC-B1P2C2A-P1-A7-DT-18	1.5	14.41	1.23	43,615
MDC-B1P2C2A-P1-A7-DT-19	NA	0.00	–	72,086*
MDC-B1P2C2A-P1-A7-EC-10	0.5	3.82	0.51	–
MDC-B1P2C2A-P1-A7-EC-11	0.5	3.76	0.55	–
MDC-B1P2C2A-P1-A7-EC-12	0.5	9.83	0.5	–
MDC-B1P2C2A-P1-A7-EC-13	0.5	9.78	0.61	–

* Failure by end brooming.

Table 7. 18-ply face sheet, 3.1 lb/ft^3 core damage tolerance results (batch 3).

Sample Name	Tup Diameter (in)	Impact Energy (ft-lb)	IRT Width (in)	Failure Stress (psi)
MDC-B1P3C3A-P1-A7-DT-1	0.25	1.62	0.36	65,814
MDC-B1P3C3A-P1-A7-DT-2	0.25	3.69	0.41	56,379
MDC-B1P3C3A-P1-A7-DT-3	0.25	5.93	0.45	51,614
MDC-B1P3C3A-P1-A7-DT-4	0.25	7.76	0.62	47,501
MDC-B1P3C3A-P1-A7-DT-5	0.25	9.73	0.65	47,239
MDC-B1P3C3A-P1-A7-DT-6	0.25	12.22	0.71	43,913
MDC-B1P3C3A-P1-A7-DT-7	0.5	3.82	0.46	56,238
MDC-B1P3C3A-P1-A7-DT-8	0.5	5.59	0.64	49,312
MDC-B1P3C3A-P1-A7-DT-9	0.5	7.64	0.54	46,685
MDC-B1P3C3A-P1-A7-DT-10	0.5	9.82	0.64	43,032
MDC-B1P3C3A-P1-A7-DT-11	0.5	11.61	0.68	44,627
MDC-B1P3C3A-P1-A7-DT-12	0.5	14.66	0.76	40,961
MDC-B1P3C3A-P1-A7-DT-13	1.5	3.74	0.53	59,296
MDC-B1P3C3A-P1-A7-DT-14	1.5	6.86	0.63	53,505
MDC-B1P3C3A-P1-A7-DT-15	1.5	7.92	0.81	49,126
MDC-B1P3C3A-P1-A7-DT-16	1.5	11.06	0.99	46,782
MDC-B1P3C3A-P1-A7-DT-17	1.5	14.23	1.28	47,355
MDC-B1P3C3A-P1-A7-DT-18	1.5	14.36	1.19	42,294
MDC-B1P3C3A-P1-A7-DT-19	NA	0.00	–	105,888*
MDC-B1P3C3A-P1-A7-EC-10	0.5	3.78	0.47	–
MDC-B1P3C3A-P1-A7-EC-11	0.5	3.76	0.58	–
MDC-B1P3C3A-P1-A7-EC-12	0.5	9.83	0.57	–
MDC-B1P3C3A-P1-A7-EC-13	0.5	9.75	0.67	–

* Failure by end brooming.

Table 8. 56-ply face sheet, 12 lb/ft^3 core damage tolerance results.

Sample Name	Tup Diameter (in)	Impact Energy (ft-lb)	PAUT Width (in)	Failure Stress (psi)
HDC-B4P1C1A-P1-A7-EC-1	0.5	20.89	0.56	76,845
HDC-B4P1C1A-P1-A7-EC-2	0.5	30.92	1.24	49,303
HDC-B4P1C1A-P1-A7-EC-3	0.5	38.36	1.06	45,841
HDC-B4P1C1A-P1-A7-EC-4	0.5	47.38	1.21	41,707
HDC-B4P1C1A-P1-A7-EC-5	0.5	54.06	1.65	40,218
HDC-B4P1C1A-P1-A7-EC-6	0.5	54.14	1.65	39,977
HDC-B4P1C1A-P1-A7-EC-7	0.5	46.77	1.77	41,496
HDC-B4P1C1A-P1-A7-EC-8	0.5	37.87	1.59	43,429
HDC-B4P1C1A-P1-A7-EC-9	0.5	30.74	1.00	52,410
HDC-B4P1C1A-P1-A7-EC-10	0.5	20.41	0.59	73,616
HDC-B4P1C1A-P1-A7-EC-11	0.5	17.47*	0.50	>78,000
HDC-B4P1C1A-P1-A7-EC-12	0.5	11.40	0.62	>78,001
HDC-B4P1C1A-P1-A7-EC-13	0.5	67.60*	2.12	35,981

* Values estimated from drop height due to instrumentation error.

Table 8 includes the damage tolerance test results for the $(45,90,-45,0)_{7s}$ 56-ply face sheet with 12 lb/ft^3 Al core. Three sets of panels composed of three lots of core and three lots of film adhesive were fabricated in the same autoclave run. The face sheets for all three panels were from the same lot of material. Only one of the three panels was machined into coupons because two of the panels

exhibited excessive core node disbonds as evidenced by NDE. Cross-sectional analysis confirmed the node disbonds. Subsequent stress analysis confirmed high residual stresses incurred within the Al core during autoclave cooldown as a result of coefficient of thermal expansion mismatch between the face sheet and core. Tensile stress on the core node bondline is a function of foil thickness. Finite element analysis predicted twice the tensile stress in the node bond for the 12 lb/ft^3 core compared to the 6.1 lb/ft^3 core. Average tensile stress estimates across the node bondline were 2,300 psi average for 12 lb/ft^3 core and 1,100 psi for 6.1 lb/ft^3 core. When modeled with a fillet at each bend in the core, the average tensile stresses were reduced. However, the discrepancy in magnitude between the different foil thicknesses remained. The failure illustrates the importance of process development as well as multiple batch testing—batch 1 core did not exhibit the disbonds. It is recommended that Al core with a foil thickness as great as the 12 lb/ft^3 material not be used in co-cure applications with carbon fiber face sheets. Figure 11 illustrates the stress model on the node bondline.
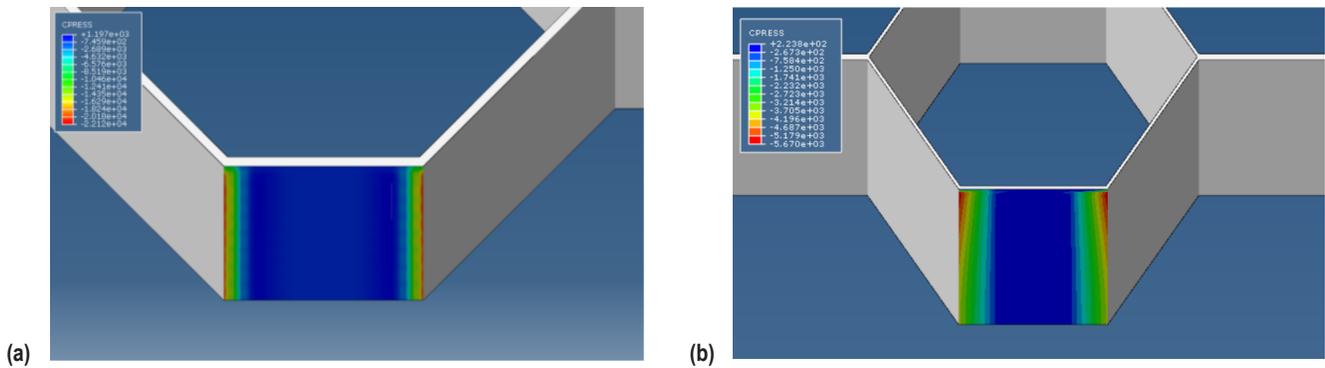

(a) **(b)**

Figure 11. Finite element analysis model of residual thermally induced stresses in (a) 12 lb/ft^3 core and (b) 6.1 lb/ft^3 core.

APPENDIX B—CROSS SECTIONS OF IMPACT DAMAGE

Figures 12–24 are cross sections of the NDE correlation panel. The 18-ply sandwich panels were impacted at energy levels from 1 to 10 ft-lb. A replicate of each impact was conducted with both 0.5- and 1.5-in-diameter impactors. Two important observations regarding the induced damage were observed. First, the larger diameter impactor created a longer delamination than the smaller diameter impactor. Second, the damage induced by the smaller diameter impactor appeared to be more widespread through the thickness of the laminate than the damage induced by the larger diameter impactor.
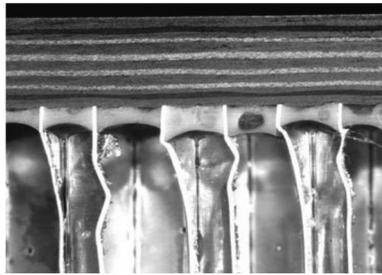
Figure 12. 1 ft-lb, 0.5-in-diameter impactor (no delamination).
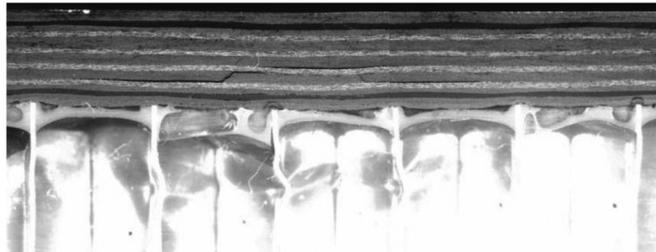
Figure 13. 2 ft-lb, 0.5-in-diameter impactor.
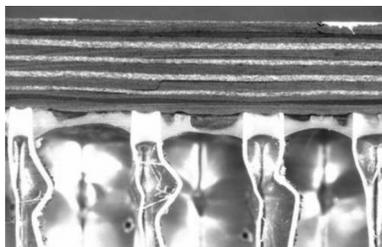
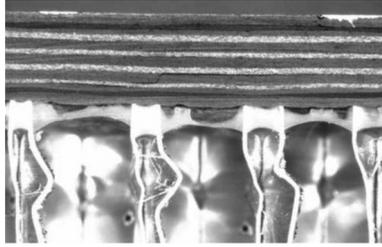Figure 14. 2 ft-lb, 1.5-in-diameter impactor.

Figure 15. 3 ft-lb, 0.5-in-diameter impactor.
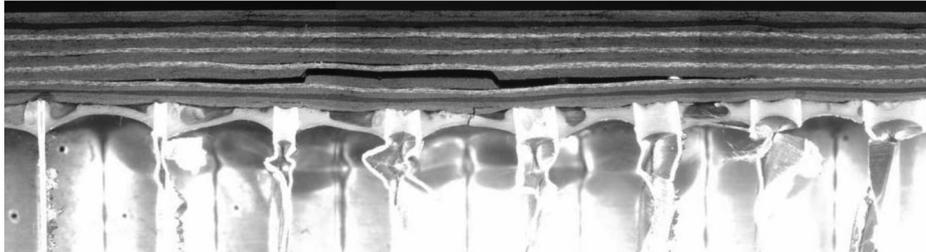

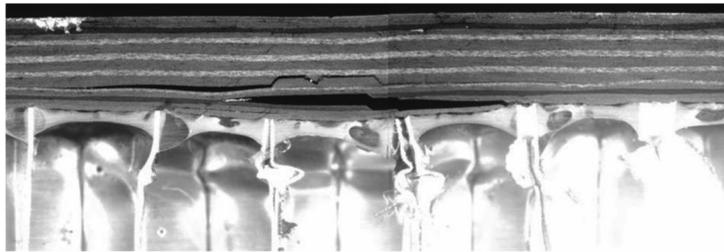Figure 16. 3 ft-lb, 1.5-in-diameter impactor.
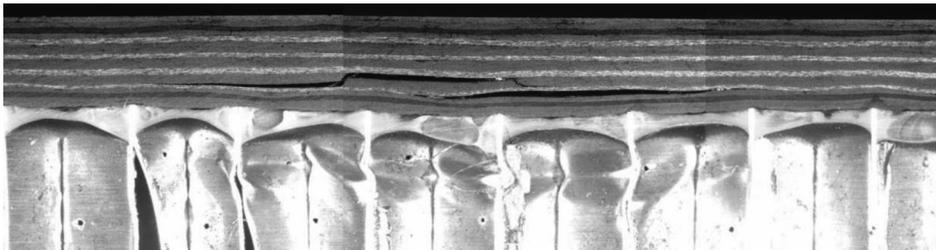

Figure 17. 4 ft-lb, 0.5-in-diameter impactor.

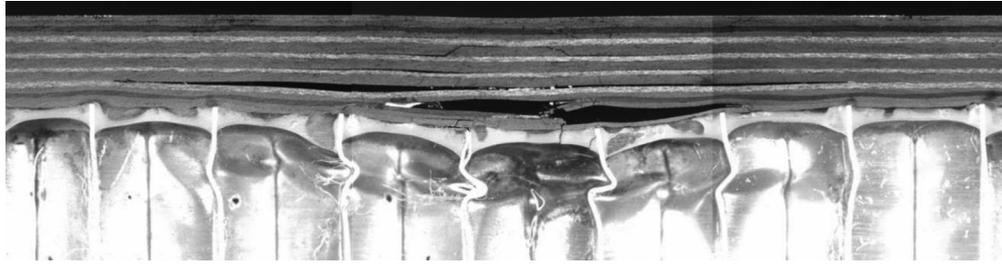Figure 18. 4 ft-lb, 1.5-in-diameter impactor.

19

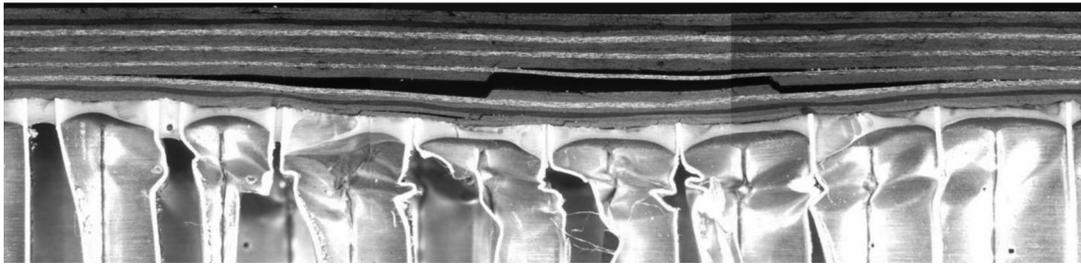Figure 19. 6 ft-lb, 0.5-in-diameter impactor.

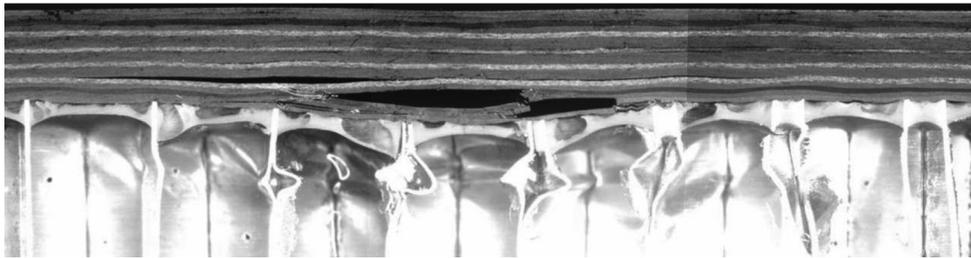Figure 20. 6 ft-lb, 1.5-in-diameter impactor.

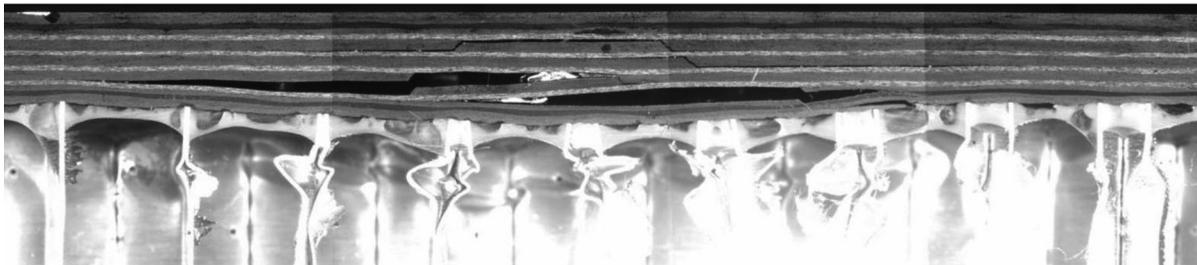Figure 21. 8 ft-lb, 0.5 in-diameter impactor.

Figure 22. 8 ft-lb, 1.5 in-diameter impactor.

20

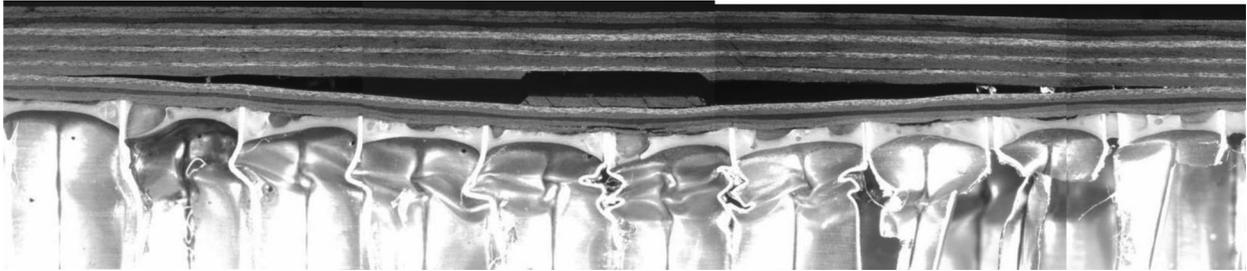Figure 23. 10 ft-lb, 0.5 in-diameter impactor.

Figure 24. 10 ft-lb, 1.5-in-diameter impactor.

REFERENCES

1. Dorey, G.: "Impact and Crashworthiness of Composite Structures," *Structural Impact and Crashworthiness*, Vol. 1, J. Morton (ed.), Elsevier Applied Science Publishers, London and New York, 1984.

2. Cantwell, W.; Curtis, P.; and Morton, J.: "Post-Impact Fatigue Performance of Carbon Fibre Laminates with Non-Woven and Mixed-Woven Layers," *Composites*, Vol. 14, No. 3, pp. 301–305, July 1983.

3. Dorey, G.: "Impact Damage in Composites—Development, Consequences and Prevention," *Proceedings, Sixth International Conference on Composite Materials, Second European Conference on Composite Materials*, Vol. 3, pp. 3.1–3.26, 1986.

4. Morton, J.; and Godwin, E.W.: "Impact Response of Tough Carbon Fibre Composites," *Compos. Struct.*, Vol. 13, pp. 1–19, 1989.

5. Bishop, S.M.: "The Mechanical Performance and Impact Behavior of Carbon-Fibre Reinforced PEEK," *Compos. Struct.*, Vol .3, pp. 295–318, 1985.

6. Cantwell, W.J.; Curtis, P.T.; and Morton J.: "An Assessment of the Impact Performance of CFRP Reienforced with High-Strain Carbon Fibers," *Compos. Sci. Technol.*, Vol. 25, pp. 133–148, 1986.

7. Whitney, J.M.; and Nuismer, R.J.: "Stress Fracture Criteria for Laminated Composites Containing Stress Concentrations," *J. Compos. Mater.*, Vol. 8, pp. 253–265, 1974.

8. Pipes, B.R.; Wetherhold, R.C.; and Gillespie, J.W., Jr.: "Notched Strength of Composite Materials," *J. Compos. Mater.*, Vol. 13, pp. 148–160, April 1979.

9. Soutis, C.; Fleck, N.A.; and Smith, P.A.: "Failure Prediction Technique for Compression Loaded Carbon Fibre-epoxy Laminate With Open Holes," *J. Compos. Mater.*, Vol. 25, pp. 1476–1498, November 1991.

10. Chen, P.; Shen, Z.; and Wang, J.Y.: "Prediction of the Strength of Notched Fiber-Dominated Composite Laminates," *Compos. Sci. Technol.*, Vol. 61, No. 9, pp. 1311–1321, July 2001.

11. Callus, P.J.: "The Effects of Hole-size and Environment on the Mechanical Behaviour of a Quasi-isotropic AS4/3501-6 Laminate in Tension, Compression and Bending," Austrailian Government Department of Defense, DSTO-TR-2077, November 2007.

12. Byers, B.A.: "Behavior of Damaged Graphite/Epoxy Laminates Under Compressive Loading," *NASA Contractor Report 159293*, Marshall Space Flight Center, AL, August 1980.

13. Williams, J.G.: "Effect of Impact Damage and Open Holes on the Compressive Strength of Tough Resin/High Strain Fiber Laminates," *NASA Technical Memorandum 85756*, Marshall Space Flight Center, AL, February 1984.

14. Chen, P.; Shen, Z.; and Wang, J.-Y.: "A New Method for Compression After Impact Strength Prediction of Composite Laminates," *J. Compos. Mater.*, Vol. 36, No. 5, pp. 589–610, 2002.

15. Edgren, F.; Asp, L.E.; and Bull, P.H.: "Compressive Failure of Impacted NCF Composite Sandwich Panels—Characterization of the Failure Process," *J. Compos. Mater.,* Vol. 38, No. 6, pp. 495–514, 2004.

16. Adams, D.F.: "Open Hole Compression Testing," *High Perform. Compos.*, pp. 12–13, March 2005.

17. ASTM D7137, Standard Test Method for Compressive Residual Strength Properties of Damaged Polymer Matrix Composite Plates, 2007.

18. Carlsson, L.A.; and Pipes, B.R.: *Experimental Characterization of Advanced Composite Materials,* 2nd Ed., Technomic Publishing Company, Inc., pp. 129–141, 1997.

19. Caprino, G.: "Residual Strength Prediction of Impacted CFRP Laminates," *J. Compos. Mater.,* Vol. 18, pp. 508–518, 1984.

20. Jenq, S.T.; Wang, S.B.; and Sheu, L.T.: "A Model for Predicting the Residual Strength of GFRP Laminates Subject to Ballistic Impact," *J. Reinf. Plast. Compos.*, Vol. 11, pp. 1127–1141, 1992.

21. Nettles, A.T.; and Jackson, J.R.: "Compression After Impact Testing of Sandwich Composites for Usage on Expendable Launch Vehicles," *J. Compos. Mater.,* Vol. 44, pp. 707–738, 2010.

REPORT DOCUMENTATION PAGE			*Form Approved* OMB No. 0704-0188

The public reporting burden for this collection of information is estimated to average 1 hour per response, including the time for reviewing instructions, searching existing data sources, gathering and maintaining the data needed, and completing and reviewing the collection of information. Send comments regarding this burden estimate or any other aspect of this collection of information, including suggestions for reducing this burden, to Department of Defense, Washington Headquarters Services, Directorate for Information Operation and Reports (0704-0188), 1215 Jefferson Davis Highway, Suite 1204, Arlington, VA 22202-4302. Respondents should be aware that notwithstanding any other provision of law, no person shall be subject to any penalty for failing to comply with a collection of information if it does not display a currently valid OMB control number.
PLEASE DO NOT RETURN YOUR FORM TO THE ABOVE ADDRESS.

1. REPORT DATE *(DD-MM-YYYY)* 01–03–2011	2. REPORT TYPE Technical Publication		3. DATES COVERED *(From - To)*
4. TITLE AND SUBTITLE Comparison of Open-Hole Compression Strength and Compression After Impact Strength on Carbon Fiber/Epoxy Laminates for the Ares I Composite Interstage			5a. CONTRACT NUMBER
			5b. GRANT NUMBER
			5c. PROGRAM ELEMENT NUMBER
6. AUTHOR(S) A.J. Hodge, A.T. Nettles, and J.R. Jackson			5d. PROJECT NUMBER
			5e. TASK NUMBER
			5f. WORK UNIT NUMBER
7. PERFORMING ORGANIZATION NAME(S) AND ADDRESS(ES) George C. Marshall Space Flight Center Marshall Space Flight Center, AL 35812			8. PERFORMING ORGANIZATION REPORT NUMBER M–1309
9. SPONSORING/MONITORING AGENCY NAME(S) AND ADDRESS(ES) National Aeronautics and Space Administration Washington, DC 20546–0001			10. SPONSORING/MONITOR'S ACRONYM(S) NASA
			11. SPONSORING/MONITORING REPORT NUMBER NASA/TP—2011–216460
12. DISTRIBUTION/AVAILABILITY STATEMENT Unclassified-Unlimited Subject Category 24 Availability: NASA CASI (443–757–5802)			
13. SUPPLEMENTARY NOTES Prepared by the Materials and Processes Laboratory, Engineering Directorate			

14. ABSTRACT

Notched (open hole) composite laminates were tested in compression. The effect on strength of various sizes of through holes was examined. Results were compared to the average stress criterion model. Additionally, laminated sandwich structures were damaged from low-velocity impact with various impact energy levels and different impactor geometries. The compression strength relative to damage size was compared to the notched compression result strength. Open-hole compression strength was found to provide a reasonable bound on compression after impact.

15. SUBJECT TERMS

composites, sandwich structures, impact damage, open-hole compression, residual strength

16. SECURITY CLASSIFICATION OF:			17. LIMITATION OF ABSTRACT	18. NUMBER OF PAGES	19a. NAME OF RESPONSIBLE PERSON STI Help Desk at email: help@sti.nasa.gov
a. REPORT	b. ABSTRACT	c. THIS PAGE	UU	32	
U	U	U			19b. TELEPHONE NUMBER *(Include area code)* STI Help Desk at: 443–757–5802

National Aeronautics and
Space Administration
IS20
George C. Marshall Space Flight Center
Marshall Space Flight Center, Alabama
35812